MODELLING OF CMOS AMS 0.35 μm N-DIFFUSION PHOTODIODE BEHAVIOUR

A. DRĂGULINESCU[1], L. LIZARRAGA[2], S. MIR[3], G. SICARD[4], O. IANCU[5]

În această lucrare prezentăm modelarea comportării unei fotodiode CMOS cu difuzie de tip n realizată printr-un proces CMOS AMS 0.35 μm. Am simulat, folosind programele T-CAD, comportarea curentului fotogenerat şi a curentului de întuneric al fotodiodei, iar apoi am comparat rezultatele cu cele provenite dintr-un model comportamental al dispozitivului (Verilog-A). Rezultatele la care am ajuns în urma celor două tipuri de simulări sunt foarte asemănătoare şi, prin urmare, putem conchide că rezultatele obținute folosind simulările de mai mare precizie realizate cu T-CAD confirmă datele din modelul Verilog-A.

In this paper we present the modelling of the behaviour of a CMOS n-diffusion photodiode that uses a CMOS AMS 0.35 μm process. We simulated with T-CAD tools the behaviour of the photogenerated current and of the dark current of the photodiode and we compared the results with those from a behavioural model of the device (Verilog-A). The results from the two simulations are very similar, and thus the results obtained with the more precise T-CAD simulations confirmed the data from the Verilog-A model.

Keywords: CMOS n-diffusion photodiode, CMOS AMS 0.35 μm process, T-CAD tools, Verilog-A model.

1. Introduction

In the latest years, CMOS image sensors (and particularly the APS sensors) have become competitors for the CCD image sensors, primarily due to their advantages, such as no blooming, simpler driving requirements and the potential of on-chip integration of sensor, analog signal conditioning circuits, A/D converter and digital processing functions. Furthermore, CMOS sensors are the best choices for low-cost imaging systems. Recently, an image identification system based on CMOS image sensor was fabricated to identify the seal images that include fingerprint, and then determine whether the seal is fake or not. The

[1] Assist., Dept. of Electronic Technology and Reliability, University POLITEHNICA of Bucharest, Romania, e-mail: dragulinescu@yahoo.com;
[2] Eng., TIMA Laboratory, Grenoble, France;
[3] Eng., TIMA Laboratory, Grenoble, France;
[4] Reader., Univ. Joseph Fourier, Grenoble, France;
[5] Prof., Dept. of Electronic Technology and Reliability, University POLITEHNICA of Bucharest, Romania.

system consisted of a colour CMOS image sensor (OV2610), a buffer memory, a CPLD, a MCU (P89C61X2), a USB2.0 interface chip (ISP1581) and a personal computer. The CPLD implement the logic and timing of the system. The MCU and the USB2.0 interface chip deal with the communications between the images acquisition system and PC. Thus PC can send some parameters and commands to the images acquisition system and also read image data from it. The identification of the images of seal is processed by the PC [1].

Another interesting application of CMOS image sensors is for retina stimulation. Degenerative photoreceptor diseases, such as age-related macular degeneration and retinitis pigmentosa, are the most common causes of blindness in the western world. A potential cure is to use a microelectronic retinal prosthesis to provide electrical stimulation to the remaining healthy retinal cells. Recently, a prototype CMOS Active Pixel Sensor was described; the device is capable of detecting a visual scene and translating it into a train of electrical pulses for stimulation of the retina. The sensor consists of a 10 x 10 array of 100 micron square pixels fabricated on a 0.35 micron CMOS process. Light incident upon each pixel is converted into output current pulse trains with a frequency related to the light intensity. These outputs are connected to a biocompatible microelectrode array for contact to the retinal cells. The flexible design allows experimentation with signal amplitudes and frequencies in order to determine the most appropriate stimulus for the retina. Neural processing in the retina can be studied by using the sensor in conjunction with a Field Programmable Gate Array (FPGA) programmed to behave as a neural network. The sensor has been integrated into a test system designed for studying retinal response [2].

Optical and potential dual imaging CMOS sensor for bioscientific applications were also proposed and fabricated. This CMOS image sensor has the capability to simultaneously capture optical and on-chip potential images. The target applications of the sensor are; 1) on-chip DNA (and other biomolecular) sensing and 2) on-chip neural cell imaging. The sensor was fabricated using a 0.35 μm 2-poly, 4-metals standard CMOS process. The sensor has a pixel array that consists of alternatively aligned optical sensing pixels (88×144) and potential sensing pixels (88×144). The total size of the array is QCIF (176×144). The size of the pixel is 7.5 μm ×7.5 μm. By choosing an appropriate operating sequence and off-chip configuration, the sensor can be operated in either a wide-range potential imaging mode (>5 V) or a high-resolution potential imaging mode (1.6mV). The sensor is applicable for most of the target applications and is capable of detecting a pH change in the solution placed on the surface. Two-dimensional optical and potential dual imaging was successfully demonstrated, and the profile of a potential spot smaller than 50 μm was clearly observed [3,4].

An experimental single-chip color HDTV image acquisition system using 8M-pixel CMOS image sensor was also developed recently. The sensor has 3840

× 2160 effective pixels and is progressively scanned at 60 frames per second. The color filter array and interpolation method to improve image quality with a high-pixel-count single-chip sensor were described. An experimental image acquisition system used to measured spatial frequency characteristics in the horizontal direction was also described. The results indicate good prospects for achieving a high quality single chip HDTV camera that reduces pseudo signals and maintains high spatial frequency characteristics within the frequency band for HDTV [5].

On-die optics is an attractive way of reducing package size for imaging and non-imaging optical sensors. While systems incorporating on-die optics have been built for imaging and spectral analysis applications, these have required specialized fabrication processes and additional off-die components. Recently the fabrication of an image sensor with neither of these limitations was discussed. Through careful design, an image sensor was implemented that uses on-die diffractive optics fabricated using a standard 0.18 micron bulk CMOS process, with simulations indicating that the resulting die is capable of acting as a standalone imaging system resolving spatial features to within 0.15 radian and spectral features to within 40 nm wavelength accuracy [6].

In this paper we present the modelling of the behaviour of a CMOS n-diffusion photodiode that uses a CMOS AMS 0.35 μm process. We will present the simulation of the photocurrent and of the dark current of the photodiode and we will compare the data extracted from T-CAD simulation programs with a behavioural model of the photodiode (Verilog-A).

2. Study of the photodiode behaviour using Verilog-A

For the behavioural model of the photodiode, we chose Verilog-A hardware description language. Verilog-A is a language derived from standard Verilog, and additionally permits the modelling of analogue and mixed-modes systems. Choosing Verilog-A was justified by its implementation in the available Cadence design environment.

Most of the values used for studying the behaviour of the diode are parameterisable, so that the model can be used to simulate other structures, after performing some modifications. Anyhow, the model is valid only for $\lambda = 565\ nm$, due to the values of the absorption coefficient and to the simplifications that were performed.

The model of the photodiode has four terminals:

- the cathode and the anode – the electrical terminals of the diode
- the light intensity - the input that sets the intensity of the incident light
- the temperature - the input that sets the temperature of the diode

The scheme of the model is presented below:

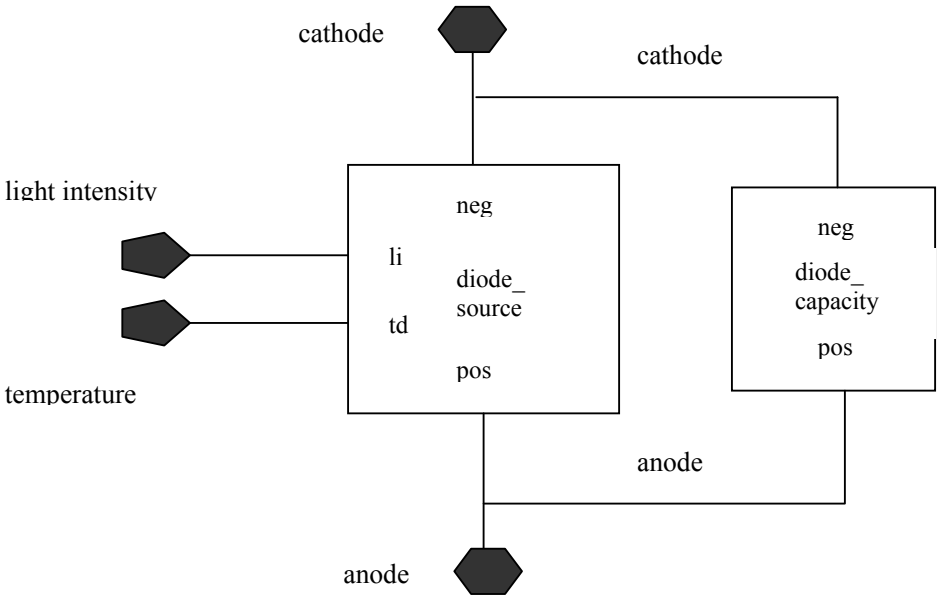

Fig. 1 The scheme of the photodiode model

The model of the diode consists in two parts: the current source (see diode_source in Fig. 1) and the variable capacity (see diode_capacity in Fig. 1).

Each block is described in Verilog-A language.

3. Study of the photodiode behaviour using T-CAD tools

The behaviour of the photodiode can be modelled mainly by the photocurrent and the dark current of the device. Next we present the simulations we made for these two characteristics.

The photocurrent was simulated by using the LUMINOUS simulator, a component of ATLAS (a very powerful tool made by the company Silvaco). We simulated the intensity for low and high levels of the illumination, respectively.

The diode was exposed to a light flux ranging from 3 to 13 nW/cm^2. The results are presented in Table 1.

Table 1

Results for the photodiode for low light levels

Incident light intensity (Illumination) $[nW/cm^2]$	Source photocurrent [fA]	Available photocurrent [fA]	Cathode current [fA]	Anode current (Photoresponse) [fA]
3	0.0820	0.0668	-2.932	2.893
5	0.1367	0.1114	-2.942	2.900
7	0.1914	0.1559	-2.953	2.938
9	0.2461	0.2005	-2.969	2.937
11	0.3008	0.2450	-3.080	3.032
13	0.3554	0.2896	-3.095	3.046

In Table 1, the source photocurrent is the equivalent current that the photodetector would produce if the energy of the beam of the source were collected with a quantum efficiency of one (= maximum). The available photocurrent represents the part of the source photocurrent that is in fact absorbed in the material regions (that is, the available photocurrent takes into account every reflexion on the lateral sides and every radiative energy loss on the backside).

Fig. 2 presents the obtained current response for the photodiode.

From Fig. 2 it can be seen that the photocurrent variations are very small (for a variation with almost an order of magnitude of the light intensity, the photocurrent varies only with approx. 0.1 fA). This can be explained by the very small light intensity (illumination).

For low light levels, the precision of ATLAS simulation is absolutely insufficient, because although ATLAS allows measurements of currents down to a level of between about $10^{-12} A/\mu m$ to $10^{-16} A/\mu m$, such values (and our values for light level are included in this range) are subject to significant numerical noise, due to the fact that the dark current has also values around these levels, and therefore the precision is poor. In order to overcome this problem, we performed a higher light intensity simulation.

The diode was exposed to a light flux ranging from 20 to 120 $\mu W/cm^2$. The results are presented in Table 2.

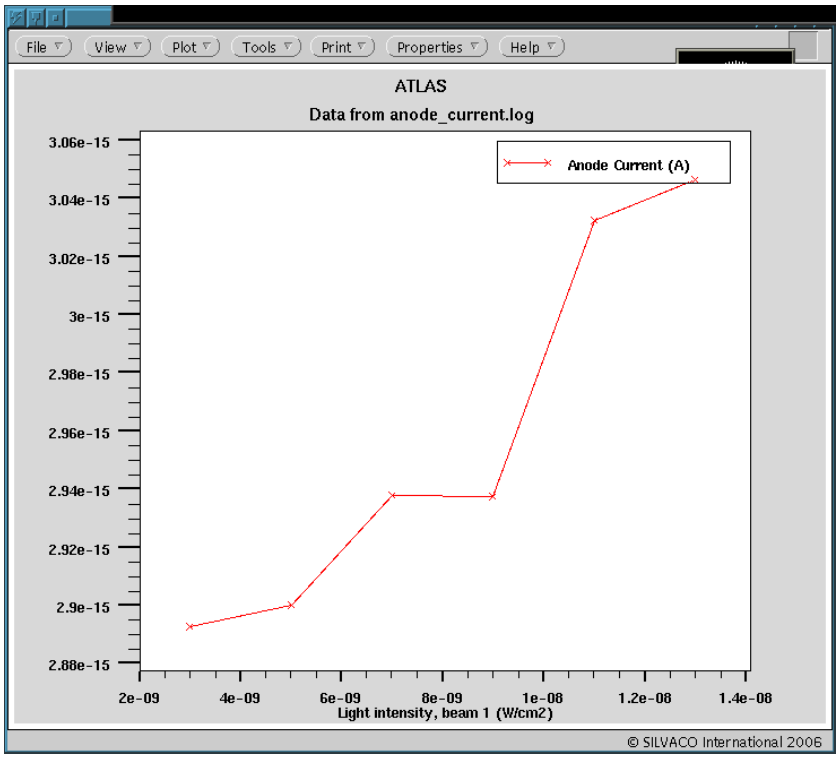

Fig. 2 Anode current (photocurrent) versus light intensity (illumination) for low light levels of the latter

Table 2

Results for the photodiode for high light levels

Illumination [$\mu W / cm^2$]	Source photocurrent [pA]	Available photocurrent [pA]	Cathode current [pA]	Anode current (Photoresponse) [pA]
20	0.5468	0.4455	-0.2693	0.2696
40	1.094	0.8910	-0.5363	0.5362
60	1.641	1.337	-0.8033	0.8032
80	2.187	1.782	-1.070	1.070
100	2.734	2.228	-1.337	1.337
120	3.281	2.673	-1.604	1.604

Fig. 3 presents the obtained current response for the photodiode.

From Fig. 3 it can be seen that the photocurrent varies significantly with the illumination, and has much higher values than in the case of low light illumination, and thus much higher than the dark current, increasing the precision of these results.

The simulation of the dark current in device simulators presents some numerical difficulties, associated with the limitations of the numerical precision. ATLAS, like most of the other available device simulators, uses double-precision arithmetic to evaluate terminal currents. Double precision arithmetic provides roughly 16 decimal digits of precision. With the internal scaling performed in ATLAS, this fact enables us to measure currents of values down to a level between $10^{-12} A/\mu m$ and $10^{-16} A/\mu m$. Unfortunately, also the values of the dark current are usually around these values. This means that the currents resulted from ATLAS are subject to a significant numerical noise, and therefore an accurate estimation of the dark current is not possible. In order to overcome this problem, there is a way of estimating the dark current, which is described below.

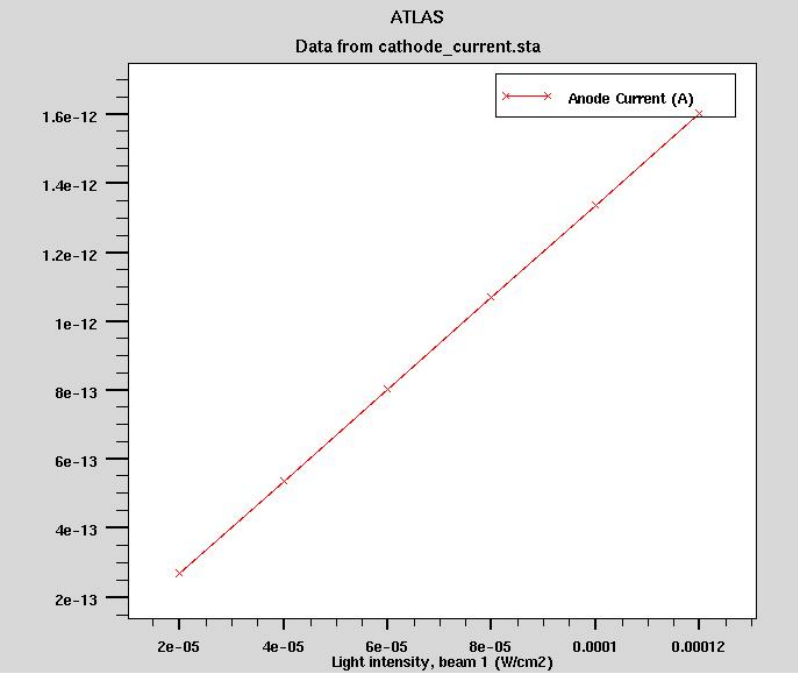

Fig. 3 Anode current (photocurrent) versus light intensity (illumination) for high light levels of the latter

From a theoretical point of view, the behaviour of the diode in reverse bias (and thus also the dark current) can be dominated by one of two effects:

- the diffusion dark currents in the neutral regions, or
- the recombination dark currents inside the depletion region.

ATLAS can provide an analysis of both mechanisms.

ATLAS can measure directly the recombination dark current, by using the instruction MEASURE to calculate the integrated recombination rate:

measure u.total

When ATLAS runs this line, it prints the total recombination rate. The user must multiply this value with the charge of the electron ($1.6 \cdot 10^{-19} C$) in order to obtain an estimation of the recombination current contribution to the leakage current of the diode in reverse bias (= to the dark current of the photodiode).

The contribution of the diffusion dark current can be estimated using the nonlinear behaviour of the diffusion dark current with temperature:

$$J = \left(\frac{q \cdot D_p \cdot P_{n_0}}{L_p} + \frac{q \cdot D_n \cdot N_{p_0}}{L_n} \right) \cdot \left[\exp\left(\frac{q \cdot V}{k \cdot T} \right) - 1 \right] \quad (1)$$

where: q – the elementary charge, in [C]

D_p / D_n - hole/electron diffusion coefficient as a minority charge, in [m^2 / s]

P/N – acceptor/donor doping

n_0 / p_0 - initial electron/hole concentration

L_p / L_n - hole/electron diffusion length as a minority charge

V – reverse bias voltage, in [V]

k - Boltzmann's constant

T – temperature, in [K]

We can write equation (1) in the following form:

$$J \cong C \cdot \exp\left(-\frac{E_g}{k \cdot T} \right) \cdot \left[\exp\left(\frac{q \cdot V}{k \cdot T} \right) - 1 \right] \quad (2)$$

where C is a multiplication constant.

From the last equation we can see that the relation of the diffusion dark current with temperature is exponential. This relation (2) can be used to estimate the contribution of the diffusion current to the total dark current. The main idea is to calculate the current at a higher temperature where the problem of the numerical precision doesn't arise, and then to scale the current at the operating temperature by using equation (2). For example, in our case the device must operate at 300 K, so we set the temperature at 450 K using the parameter TEMPERATURE from the MODEL statement. Any temperature dependence of the energy gap must be disabled by explicit specification of the bandgap, using the parameter EG300 and setting to zero the parameters EGALPHA and EGBETA[6], all in MATERIAL statement. For our silicon diode, the statements we use are:

[6] EG300 – specifies the bandgap at 300 K
EGALPHA, EGBETA – specify the parameters α and β, respectively, from the equation:

model temperature = 450
material eg300 = 1.12 egalpha = 0.0 egbeta = 0.0

Then, ATLAS can be used to obtain the diffusion dark current at that high temperature (here: 450 K). Finally, to calculate the diffusion dark current at the operating temperature (here: 300 K), we use the equation:

$$J = J_e \cdot \exp\left(\frac{E_g}{k \cdot T_e} - \frac{E_g}{k \cdot T}\right) \cdot \frac{\exp\left(\frac{q \cdot V}{k \cdot T}\right) - 1}{\exp\left(\frac{q \cdot V}{k \cdot T_e}\right) - 1} \tag{3}$$

or :

$$J = J_e \cdot \exp\left[\frac{E_g}{k} \cdot \left(\frac{1}{T_e} - \frac{1}{T}\right)\right] \cdot \frac{\exp\left(\frac{q \cdot V}{k \cdot T}\right) - 1}{\exp\left(\frac{q \cdot V}{k \cdot T_e}\right) - 1} \tag{4}$$

where: J – estimated diffusion dark current at the operating temperature T

J_e - measured diffusion dark current at the high (= elevated) temperature T_e

E_g - (silicon) energy bandgap.

Finally, the total dark current can be obtained by summing the estimations of the recombination and diffusion dark currents [11].

The results for the simulation of the diffusion dark current at 450 K and calculus of this current at 300 K are presented in Table 3.

Table 3

Diffusion dark current in the photodiode

Reverse bias [V]	Diffusion dark current at 450 K [pA]	Diffusion dark current at 300 K [fA]
3	2.449	3.109
4	2.760	3.504
5	3.221	4.089

$$E_g(T_e) = E_g(300) + \alpha \cdot \left(\frac{300^2}{300 + \beta} - \frac{T_e^{\,2}}{T_e + \beta}\right) \cdot$$

The values from the second column of the table were obtained after the simulation with ATLAS, and the values from the third column were calculated using equation (4).

The results for the simulation of the recombination dark current we obtained are presented in Table 4.

Table 4

Recombination dark current in the photodiode

Reverse bias [V]	Recombination rate $\cdot 10^5$	Recombination dark current at 300 K [fA]
3	-0.05966	1.102
4	-0.07275	1.433
5	-0.08291	1.466

The results for the total dark current of the photodiode are presented in Table 5.

Table 5

Calculated total dark current of the photodiode

Reverse bias [V]	Total dark current [fA]
3	4.211
4	4.937
5	5.555

The results were obtained by summing the values for the diffusion and recombination dark currents at 300 K.

4. Comparison between data extracted with T-CAD and Verilog-A

In order to validate the behavioural model of the photodiode, we compared the results from that model with the data obtained using T-CAD tools (ATLAS). Next we present this comparison for the photocurrent, dark current and quantum efficiency of the photodiode.

The medium value of the quantum efficiency calculated from the data obtained with ATLAS is: $\eta = 60.14\,\%$.

The value of the quantum efficiency obtained with Verilog-A is: $\eta = 66.80\,\%$.

The direct comparison between illumination response simulations performed with VerilogA and ATLAS is impossible, because the ATLAS simulator is two dimensional and it assumes that the width of the simulated structure is equal to $1\,\mu m$ (we assumed a $10\,\mu m$ long, $1\,\mu m$ wide and $14\,\mu m$ thick photodiode).

In order to make the comparison, a photodiode of $10\ \mu m$ x $10\ \mu m$ x $14\ \mu m$ was simulated with Verilog-A model, and the results obtained with ATLAS were multiplied by 10.

The comparison is presented in Fig. 4.

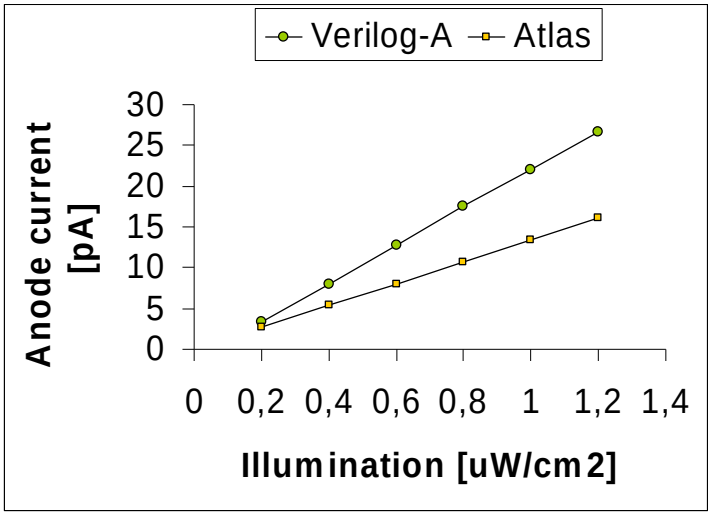

Fig. 5 shows the comparison between the simulated dark current with Verilog-A and with ATLAS.

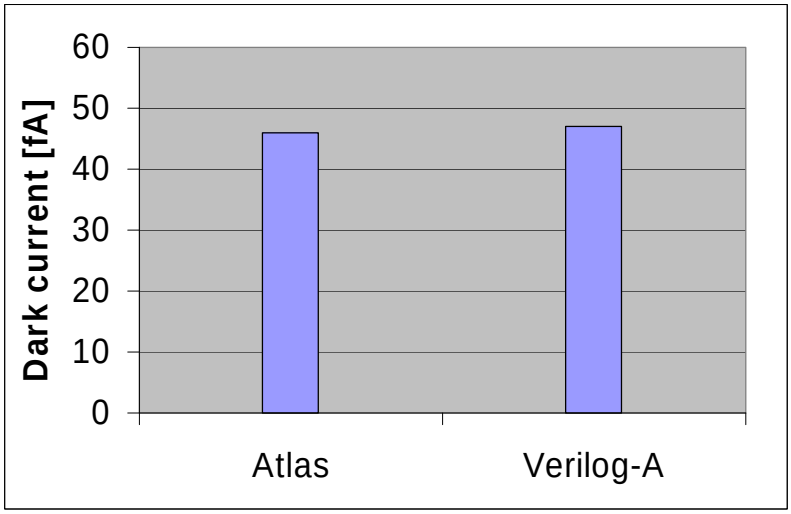

5. Conclusions

Despite of the problems created in ATLAS simulations by the unknown technology specifications, the differences between the simulations of the dark current with Verilog-A and ATLAS are quite insignificant. The results for the photocurrent are relatively similar (those for VerilogA are higher). The value we obtained for the quantum efficiency was 60.14% with ATLAS and 66.80% with Verilog A.

REFERENCES

[1] *X. Xue, S. Zhang, Y. Guo,* An image identification system of seal with fingerprint based on CMOS image sensor, in Proceedings of the SPIE, **vol. 6027**, pp. 844-851, January 2006.

[2] *M. Prydderch, M. French, K. Mathieson, C. Adams, D. Gunning, J. Laudanski, J. Morrison, A. Moodie, J. Sinclair,* A CMOS active pixel sensor for retinal stimulation, in Proceedings of the SPIE, **vol. 6068**, pp. 17-25, February 2006.

[3] *T. Tokuda, A. Yamamoto, K. Kagawa, M. Nunoshita, J. Ohta,* An optical and potential dual-image CMOS sensor for bioscientific applications, in Proceedings of the SPIE, **vol. 6068**, pp. 10-16, February 2006.

[4] *T. Tokuda, A. Yamamoto, K. Kagawa, M. Nunoshita, J. Ohta,* A CMOS image sensor with optical and potential dual imaging function for on-chip bioscientific applications, in Sensors and Actuators, A Physical, **vol. 125**, no. 2, pp. 273-280, 2006.

[5] *H. Shimamoto, T. Yamashita, R. Funatsu, K. Mitani, Y. Nojiri,* Experimental single-chip color HDTV image acquisition system with 8M-pixel CMOS image sensor, Proceedings of the SPIE, **vol. 6068**, pp. 69-76, February 2006.

[6] *C. Thomas, R. Hornsey,* An image sensor with on-die diffractive optics in 0.18µm bulk CMOS, Proceedings of the SPIE, **vol. 6068**, pp. 49-60, February 2006.

[7] *M. Marzencki,* APS system design for biochip application, Graduation Thesis, Grenoble/Cracow, 2003.

[8] *L. Lizarraga, S. Mir, G. Sicard,* Study of a BIST Technique for the CMOS Active Pixel Sensors, Proc. of VLSI-SOC, pp 326-331, June 2006.

[9] *R. Turchetta, K. Spring, M. Davidson,* Introduction to CMOS Image Sensors, Olympus America Inc., and the Florida State University, 1998 – 2006.

[10] 0.35 µm CMOS Opto Process Datasheet, Austriamicrosystems, November 2003.

[11] ATLAS User's Manual, SILVACO International, 1997.

[12] *C. Wang, C. Sodini,* Characterization of CMOS Photodiodes for Image Sensor Applications, http://www-mtl.mit.edu/researchgroups/sodini/research_report9.html.

[13] *L. Lizarraga, S.Mir, G. Sicard, A. Drăgulinescu,* Defect and Fault Modelling of CMOS Active Pixel Sensors, in LATW 2007 (8th IEEE Latin-American Test Work Shop), Cuzco, Peru, March 2007.